

Studying and Analysis of the pollutant distribution trajectory from Ethiopian volcano using HYSPLIT Code

Abstract:-

In this study, the atmospheric transport of airborne contaminants released from an Ethiopian volcanic eruption is investigated using the Hybrid Single-Particle Lagrangian Integrated Trajectory (HYSPLIT) model. This is done within the framework of environmental radiological dispersion, as defined by the United Nations Scientific Committee on the Effects of Atomic Radiation (UNSCEAR) and the International Atomic Energy Agency (IAEA). The evolution of plume transport from the initial release phase to long-range atmospheric dispersion is characterized using forward trajectory simulations, which are equivalent to the behavior of radioactive aerosols after an unintentional or unplanned release. The analysis shows that source-term characteristics, in particular buoyancy-driven plume rise and effective release height, have an impact on early plume transmission, which is in line with radiological source-term notions. Advection in the regional and synoptic-scale wind fields, vertical wind shear, and atmospheric stability are the main factors influencing atmospheric transport at later phases. The cumulative consequences of atmospheric variability and stochastic transport processes are shown in the increasing spatial dispersion and divergence of trajectories. The results validate the use of trajectory-based atmospheric transport models for evaluating the long-range dispersion, transboundary movement, and possible environmental effects of radioactive elements in the air.

Introduction:-In North East Africa, Ethiopia is 1,104,300 km² in size and borders Sudan and South Sudan to the west, Djibouti and Somalia to the east, and Eritrea to the north. Kenya to the south. The nation's climate and topography are varied, ranging from desert-like conditions in the northeast, east, and south-east lowlands to the tropical rainforest with heavy rainfall and humidity in the south and southwest to the Afro-Alpine on the summits of the Simien and Bale Mountains. Ethiopia is generally thought of as being desert, although its precipitation varies greatly. Ethiopia's climate may be broadly classified into three zones: 1) the alpine vegetation cool zones (Dega), which are found over 2,600 meters above sea level and have temperatures between 16°C and almost freezing; 2) WoinaDega's temperate zones, where a large portion of the nation's population is concentrated in places with temperatures between 16°C and 30°C that are 1,500–2,500 meters above sea level; and 3) the hot Qola zone, which includes both tropical and desert regions and has temperatures between 27°C and 50°C. An ethno-federalist system governs Ethiopia, which is divided into ten regions: Tigray, Afar, Amhara, Oromia, Somalia, Benshangul-Gumuz, Ethiopia, the second most populous country in Africa, is home to over 112 million people (2019), with an annual population growth rate of 2.6%. Other cities include Sidama, Southern Nations, Nationalities and Peoples (SNNP), Gambela, and Harari Peoples.⁴ Addis Ababa, the capital, and Dire Dawa are the two city administrations. By 2030, it is expected to have 139.6 million residents, and by 2050, 190.8 million. Due to its heavy reliance on rainfed agriculture and natural resources, as well as its comparatively low ability to adapt to these anticipated changes, Ethiopia is among the nations most vulnerable to climate variability and climate change. Underdeveloped water resources, poor health care coverage, rapid population increase, low economic development, poor road infrastructure in drought-prone areas,

shoddy institutional frameworks, and a lack of knowledge are some of the difficulties. In addition to unpredictable rainfall and rising temperatures, Ethiopia has regularly seen extreme occurrences including droughts and floods, all of which have a negative influence on livelihoods. Soil erosion, deforestation, frequent droughts, desertification, land degradation, and the extinction of species and biodiversity are the main environmental issues. Ethiopia is vulnerable to many natural disasters, such as earthquakes, floods, volcanoes [1]. Hayli Gubbi, which is situated in the Afar area of northeastern Ethiopia, erupted explosively on November 23, 2025, marking a notable geological event in Ethiopia. Since it was the first recorded explosive activity of this volcano in about 12,000 years, the eruption in November 2025 was especially noteworthy as it signaled the revival of a dormant magmatic system during the Holocene era [2-6]. The eruption produced a significant plume of ash that penetrated the upper troposphere and may have entered the lower stratosphere, rising to a height of roughly 10–14 km above sea level. Increased regional environmental impact and improved long-range atmospheric movement are linked to such plume heights. Geographically and atmospherically, the eruption emitted large amounts of volcanic ash and gasses, such as carbon dioxide (CO₂) and sulfur dioxide (SO₂) [7-11]. This study used the Hybrid Single-Particle Lagrangian Integrated Trajectory (HYSPPLIT) model [12-16].

Methodology :-

HYSPPLIT is utilized for emergency response instances as well as research applications that call for simulating the movement and dispersion of dangerous contaminants in the atmosphere. The ATD (the atmospheric transport and diffusion) modeling of pollutants and hazardous compounds, as well as the deposition of these materials onto the Earth's surface, are all supported by the model. Applications include monitoring and predicting the emission of contaminants (like mercury) from several stationary emission sources, including volcanic ash, radioactive material, and smoke from wildfires [17-18]. Either puff or particle modes can be used in HYSPPLIT to calculate a pollutant's dispersion. Additionally, there are hybrid puff/particle modes that can handle dispersion as a combination of puff and particle modes. In puff mode, puffs separate into multiple new puffs, each with its own portion of the pollutant mass, after expanding to a size greater than the meteorological grid cell (either vertically or horizontally). The particle mode uses a random turbulence component to disperse a predetermined number of particles that are advected over the model domain with the mean wind field. Dry deposition in HYSPPLIT is either clearly defined as a deposition velocity or calculated using the resistance approach [19-20] and surface characteristics. In HYSPPLIT, deposition is only calculated when the particle center location or the puff's bottom is inside the surface layer. The deposition layer next to the ground is assumed to have a uniform vertical concentration distribution in order to determine the mass deposited. After the mass has been extracted from the puff or particle, it is distributed (deposited) onto the ground. Rainfall through a polluted layer and continuous ingestion of dirty air into a cloud from a polluted boundary layer are the two types of wet deposition processes [19-20]. A scavenging coefficient is employed for pollutant elimination in rain that falls below a cloud layer, while the simplifying assumption of a scavenging ratio is applied to particulate pollutants that are found within a cloud layer. The Henry's Law coefficient of soluble gases can be used to define wet removal. Only the portion of the pollutant below the cloud top is removed by gaseous wet removal. The advection–diffusion equations regulating

atmospheric transport are solved using HYSPLIT using these inputs. The main method used by HYSPLIT is a Lagrangian particle approach, in which pollutant mass constituents are represented by individual particles. The trajectory of each particle is calculated using [21-24]:

$$\frac{d\vec{X}}{dt} = U(x,t) + U'(t)$$

Where:

$\vec{X}(t)$ = vector of particle position

U = component of deterministic wind

U' = component of stochastic turbulent velocity

The turbulent component is often parameterized as:

$$U'(t) = \sqrt{2K\Delta t} R$$

Where:

K = eddy diffusivity

Δt = time step

R = random number from a Gaussian distribution

Results and Discussion:- The air trajectory of the volcanic plume released from an Ethiopian volcano is shown in Figure (1), which also shows the routes taken by gases and volcanic ash after an eruption. High eruption temperatures create great thermal buoyancy, which causes the plume to ascend initially. When buoyant forces start to fade, large-scale air circulation takes over plume motion. It shows the early stage of the volcanic cloud's eruption from the Ethiopian volcano, and the curvature of the trajectories shows the influence of vertical wind shear and prevailing wind fields, suggesting that plume transmission is highly height-dependent. At this point, the cloud's direction is determined by the mid troposphere's wind speed. Figure (2) shows the cloud's initial forward motion shortly after eruption, with regional winds controlling the direction of transport while the cloud retains its density. Figure (3) shows the trajectories in the early post-eruption phase, when wind shear effects start to occur. There is a primary northeastward trajectory and a secondary eastward trajectory. The increased influence of vertical wind shear, which causes air parcels at slightly different heights to experience variable wind velocity and directions, is shown in the increasing distance between trajectories. Even when there isn't much turbulence, the plume is stretched both horizontally and vertically by this shear-induced deformation. The trajectories in Figure (4) exhibit curvature and distinct transport paths, becoming more and more divergent over time. The observed curvature is a clear example of synoptic-scale wind turning with height, which is

frequently linked to Coriolis forcing and pressure gradients. Even in the absence of variations in the intensity of eruptions, the plume continuously deforms as various layers are advected by various wind regimes. Plume trajectories that extend farther downwind and span a significantly greater geographic zone are shown in Figure (5). The long transmission distances show that the plume is a part of long-term, extensive circulation patterns. At this point, synoptic winds virtually control plume motion, with little any impact from nearby local meteorological factors. The trajectory envelope clearly widens in Figure (6). This widening is a result of the wind field's small-scale change over time. When combined over extended transport times, even little variations in wind direction and speed result in notable spatial dispersion. Plume paths in Figure (7) show a noticeable curvature. The plume's interaction with changing synoptic systems, including ridges or troughs, which reroute airflow at mid- and upper-tropospheric levels, causes the curvature. This impact has an entirely atmospheric origin and is unaffected by eruption feature. Figure (8) demonstrates that Ethiopian volcanic emissions have the ability to affect areas that are far from the eruption site, with plume trajectories spanning extremely great distances. Figure (9) shows several paths from the same starting point and notable directional diversity brought on by the modeling's differences in stack height. Figure 10: The routes are obviously in line with trade winds or subtropical jet streams and are connected to regional circulation systems. Figure (11): Potential deposition areas shift and the areas of influence gradually shift from a local to a distant regional scale throughout time. Figure (12): Radial propagation and significant spatial dispersion with a diminishing focal focus. Figure (13): The traces extend to regions that are quite remote from the source, such as North Africa and the Eastern Mediterranean. Figure (14): The accumulation of air contacts and lack of cohesiveness are reflected in the emission's final stages, which exhibit comparatively slow movement. Figure (15) shows randomly diverging trails due to severe air turbulence dominance and weak directional cohesiveness. Figure (16): shows the volcanic cloud's final overall track from Ethiopia to Northeast Africa. This all are because the volcanic plume is propelled into a rapid vertical rise within the troposphere by the substantial thermal buoyancy created by the exceptionally high temperatures at the time of eruption. The movement of the cloud is controlled by large-scale circulation systems as the buoyant forces eventually decrease as a result of the reduction of thermal density differences. The measured pathways' curvature, which is a reflection of vertical wind shear—the change in wind direction and speed with altitude—indicates that the vertical injection level has a significant impact on the cloud's movement. At this point, the middle troposphere winds control the main direction of movement, with horizontal advection taking center stage. While regional winds regulate the direction of travel, the air mass maintains its relative density. The observation of a primary path toward the northeast and a secondary path toward the east indicates the predominance of horizontal advection processes prior to the onset of large-scale dispersion. The variations in wind properties between various atmospheric strata are reflected in this variation. The effect of vertical shear, in which air particles at relatively near altitudes are subjected to varying wind speeds and directions, is indicated by the growing separation between the trajectories. This causes the cloud to expand both horizontally and vertically, even when there aren't any significant atmospheric disturbances. Over time, the pathways clearly diverge and show increasing curvature. This curvature, which is caused by the Coriolis force and atmospheric pressure gradients, is a well-known illustration of wind rotation on the synoptic scale. As each layer moves within a distinct wind system, the cloud continues to experience structural deformation even in the absence

of a change in the eruption's intensity. The routes span a larger geographic area and have a greater extension downwind. This suggests that the cloud has made its way into extensive, long-term circulation networks. At this point, local atmospheric influences become less significant, and synoptic winds nearly take over. It is clear that the path envelope is expanding. Little changes in the wind field's timing and location cause this expansion. The enhanced global distribution can be explained by the substantial spatial dispersion that results from these alterations building up over an extended travel period. Because the cloud interacts with different pressure systems, such as high and low pressure systems, which reroute airflow in the intermediate and higher layers of the troposphere [25-36].

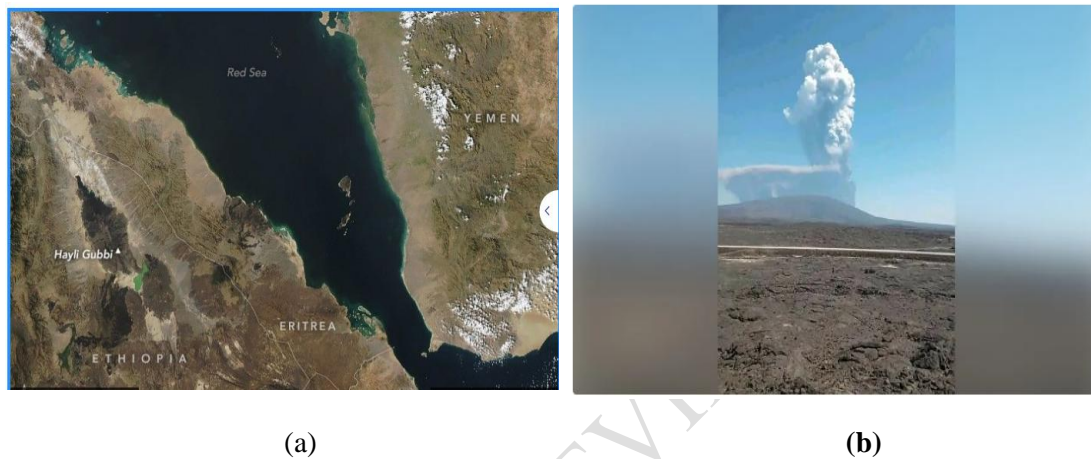


Figure (1) :-

- (a) depicts the air trajectory of the volcanic plume that was ejected from an Ethiopian volcano.
- (b) Show that Ash billows from an eruption of the long- dormant HayliGubbi Volcano in Ethiopia

NOAA HYSPLIT MODEL - TRAJECTORY FREQUENCIES
 # trajs passing through grid sq./# trajectories (%) 0 m and 99999 m
 Integrated from 1400 29 Nov to 1100 03 Dec 25 (UTC)
 Freq Release started at 0000 00 00 (UTC)

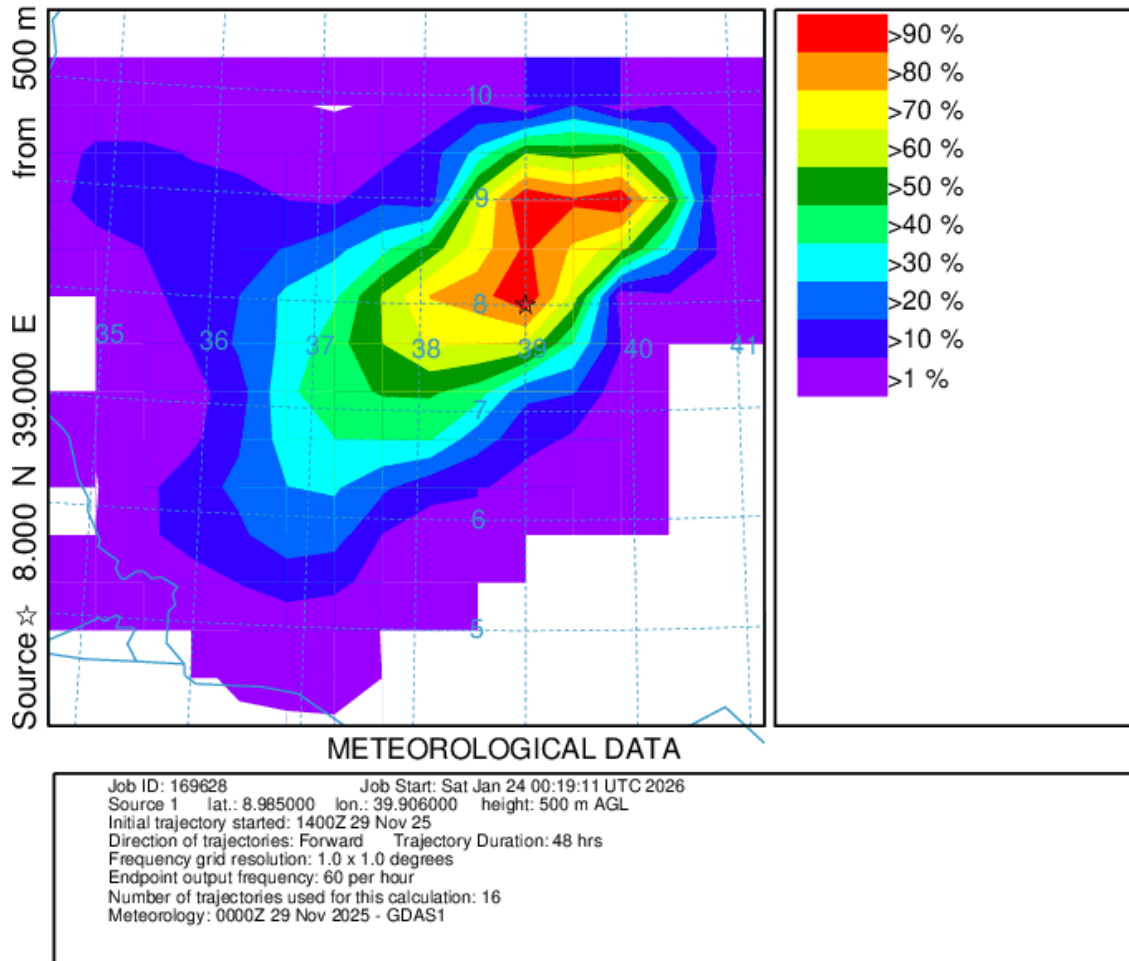
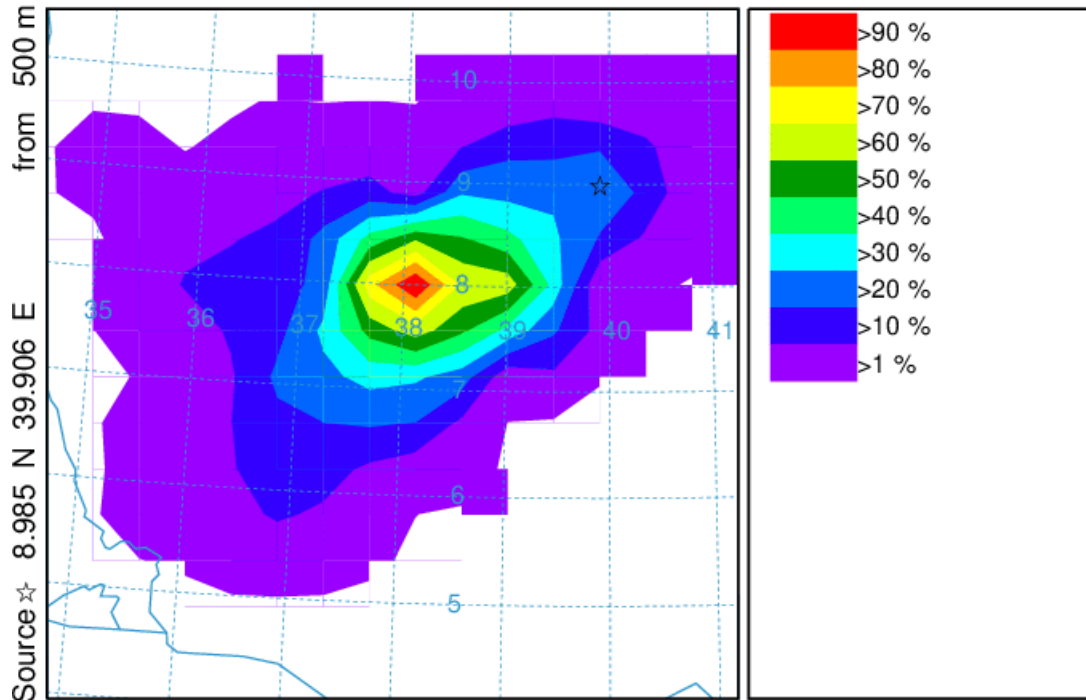


Figure (2) displays the volcanic plume's initial onward motions following the Ethiopian eruption.

NOAA HYSPLIT MODEL - TRAJECTORY FREQUENCIES
 # endpts per grid sq./max # endpts in any grid sq. (%) 0 m and 99999 m
 Integrated from 1400 29 Nov to 1100 03 Dec 25 (UTC)
 Freq Release started at 0000 00 00 (UTC)



METEOROLOGICAL DATA

Job ID: 169628 Job Start: Sat Jan 24 00:19:11 UTC 2026
 Source 1 lat.: 8.985000 lon.: 39.906000 height: 500 m AGL
 Initial trajectory started: 1400Z 29 Nov 25
 Direction of trajectories: Forward Trajectory Duration: 48 hrs
 Frequency grid resolution: 1.0 x 1.0 degrees
 Endpoint output frequency: 60 per hour
 Number of trajectories used for this calculation: 16
 Meteorology: 0000Z 29 Nov 2025 - GDAS1

Figure (3) shows the plume trajectories in the immediate aftermath of the eruption.

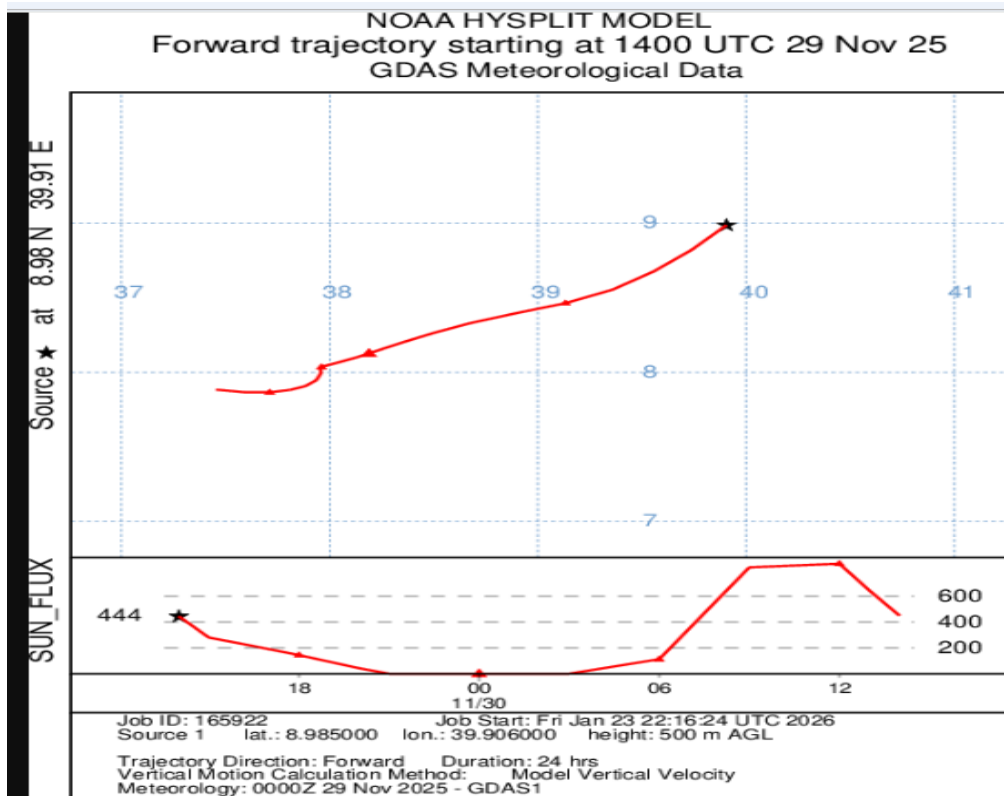
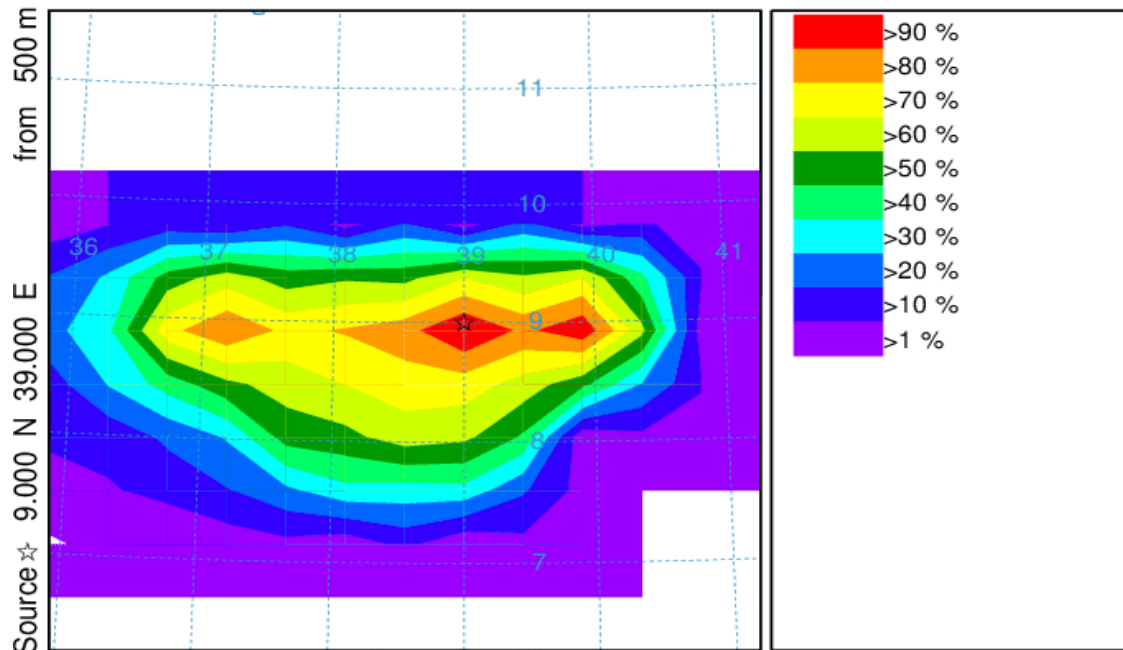


Figure (4) show increasing divergence due to curvature and separate transport pathways.

NOAA HYSPLIT MODEL - TRAJECTORY FREQUENCIES

trajs passing through grid sq./# trajectories (%) 0 m and 99999 m
Integrated from 1400 01 Dec to 1100 05 Dec 25 (UTC)
Freq Release started at 0000 00 00 (UTC)

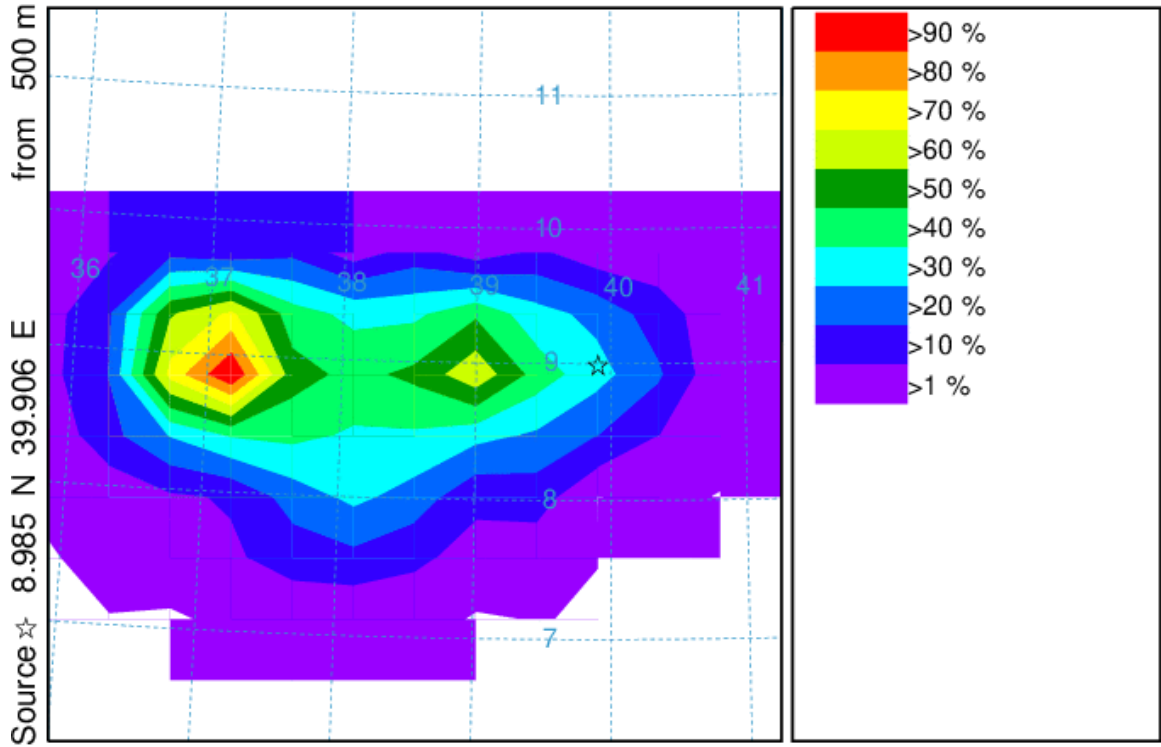


METEOROLOGICAL DATA

Job ID: 169793 Job Start: Sat Jan 24 00:24:10 UTC 2026
Source 1 lat.: 8.985000 lon.: 39.906000 height: 500 m AGL
Initial trajectory started: 1400Z 01 Dec 25
Direction of trajectories: Forward Trajectory Duration: 48 hrs
Frequency grid resolution: 1.0 x 1.0 degrees
Endpoint output frequency: 60 per hour
Number of trajectories used for this calculation: 16
Meteorology: 0000Z 1 Dec 2025 - GDAS1

Figure (5) displays plume trajectories that cover a substantially larger geographic zone

NOAA HYSPLIT MODEL - TRAJECTORY FREQUENCIES
 # endpts per grid sq./max # endpts in any grid sq. (%) 0 m and 99999 m
 Integrated from 1400 01 Dec to 1100 05 Dec 25 (UTC)
 Freq Release started at 0000 00 00 (UTC)



METEOROLOGICAL DATA

Job ID: 169793 Job Start: Sat Jan 24 00:24:10 UTC 2026
 Source 1 lat.: 8.985000 lon.: 39.906000 height: 500 m AGL
 Initial trajectory started: 1400Z 01 Dec 25
 Direction of trajectories: Forward Trajectory Duration: 48 hrs
 Frequency grid resolution: 1.0 x 1.0 degrees
 Endpoint output frequency: 60 per hour
 Number of trajectories used for this calculation: 16
 Meteorology: 0000Z 1 Dec 2025 - GDAS1

Figure (6) shows a noticeable widening of the trajectory envelope.

UNDER REVIEW

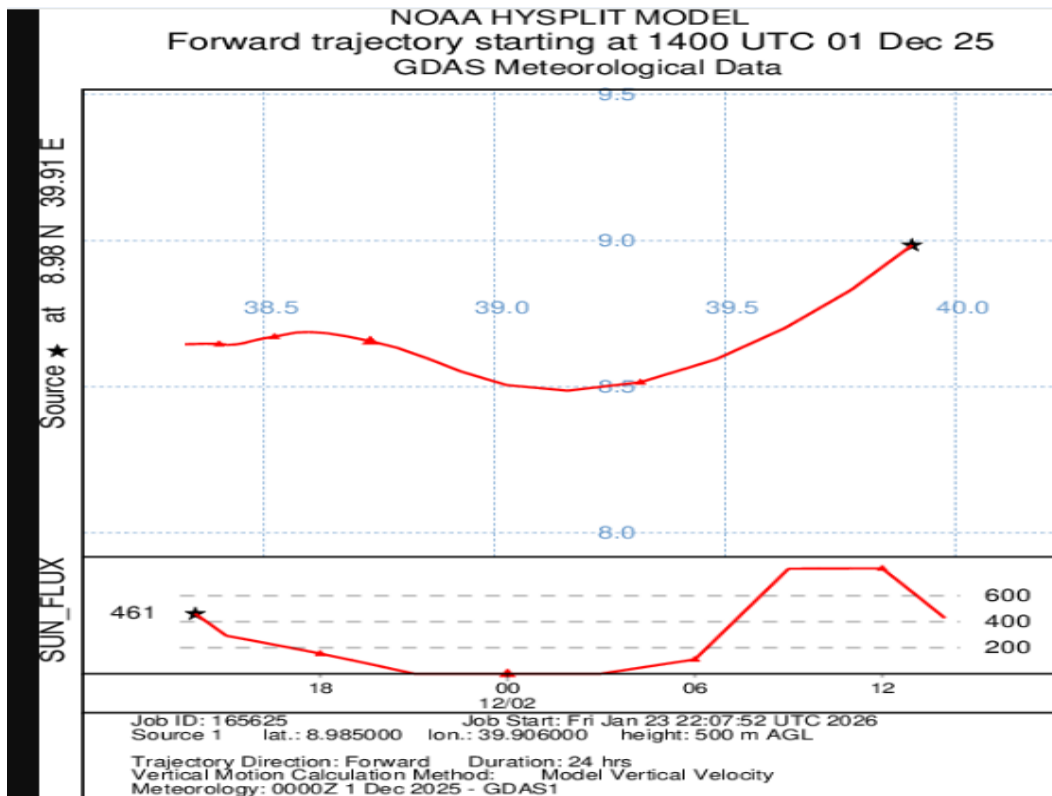
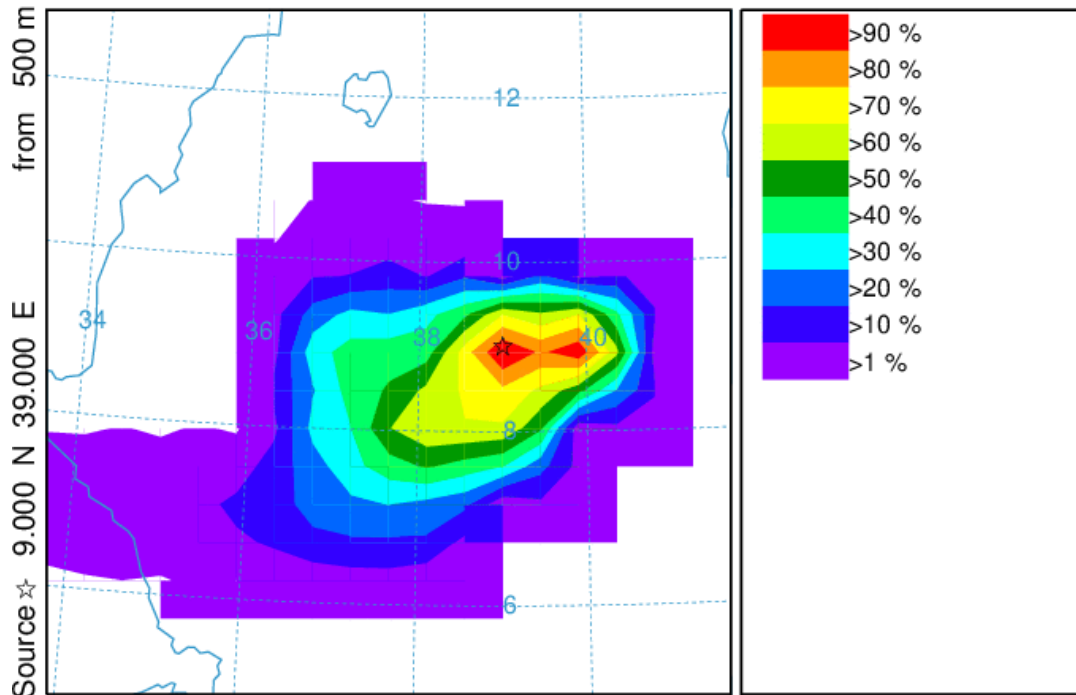


Figure (7) shows plume trajectories have a discernible curvature.

NOAA HYSPLIT MODEL - TRAJECTORY FREQUENCIES
 # trajs passing through grid sq./# trajectories (%) 0 m and 99999 m
 Integrated from 1400 08 Dec to 1100 12 Dec 25 (UTC)
 Freq Release started at 0000 00 00 (UTC)

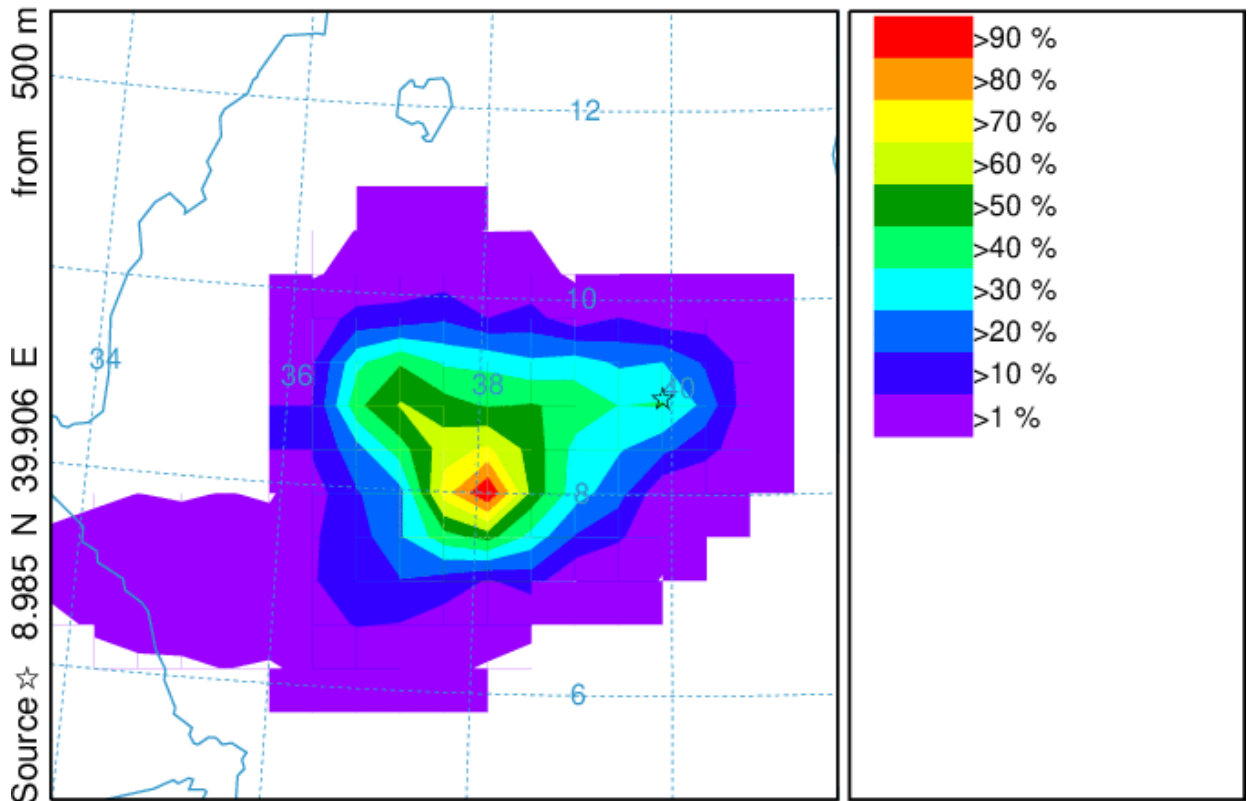


METEOROLOGICAL DATA

Job ID: 169929 Job Start: Sat Jan 24 00:29:29 UTC 2026
 Source 1 lat.: 8.985000 lon.: 39.906000 height: 500 m AGL
 Initial trajectory started: 1400Z 08 Dec 25
 Direction of trajectories: Forward Trajectory Duration: 48 hrs
 Frequency grid resolution: 1.0 x 1.0 degrees
 Endpoint output frequency: 60 per hour
 Number of trajectories used for this calculation: 16
 Meteorology: 0000Z 8 Dec 2025 - GDAS1

Figure (8) demonstrates that Ethiopian volcanic emissions from the eruption site.

NOAA HYSPLIT MODEL - TRAJECTORY FREQUENCIES
 # endpts per grid sq./max # endpts in any grid sq. (%) 0 m and 99999 m
 Integrated from 1400 08 Dec to 1100 12 Dec 25 (UTC)
 Freq Release started at 0000 00 00 (UTC)



METEOROLOGICAL DATA

Job ID: 169929 Job Start: Sat Jan 24 00:29:29 UTC 2026
 Source 1 lat.: 8.985000 lon.: 39.906000 height: 500 m AGL
 Initial trajectory started: 1400Z 08 Dec 25
 Direction of trajectories: Forward Trajectory Duration: 48 hrs
 Frequency grid resolution: 1.0 x 1.0 degrees
 Endpoint output frequency: 60 per hour
 Number of trajectories used for this calculation: 16
 Meteorology: 0000Z 8 Dec 2025 - GDAS1

Figure 9 shows a wide range of trajectories with comparable starting conditions.

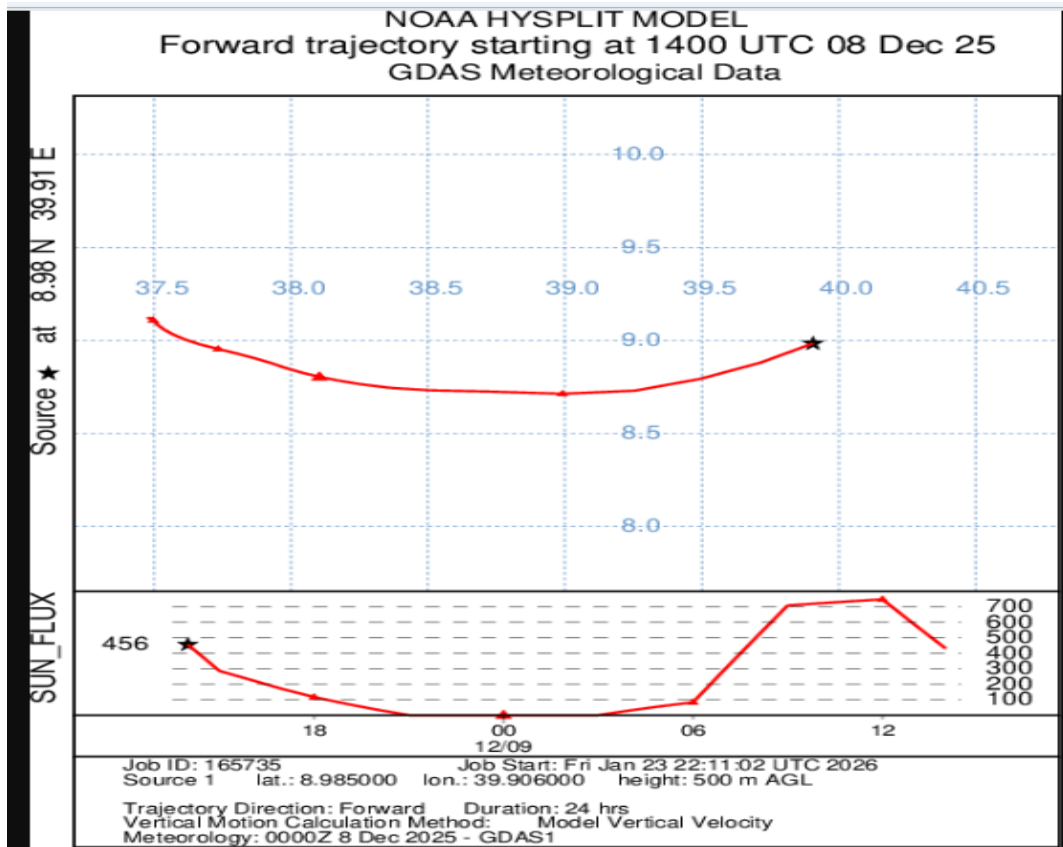
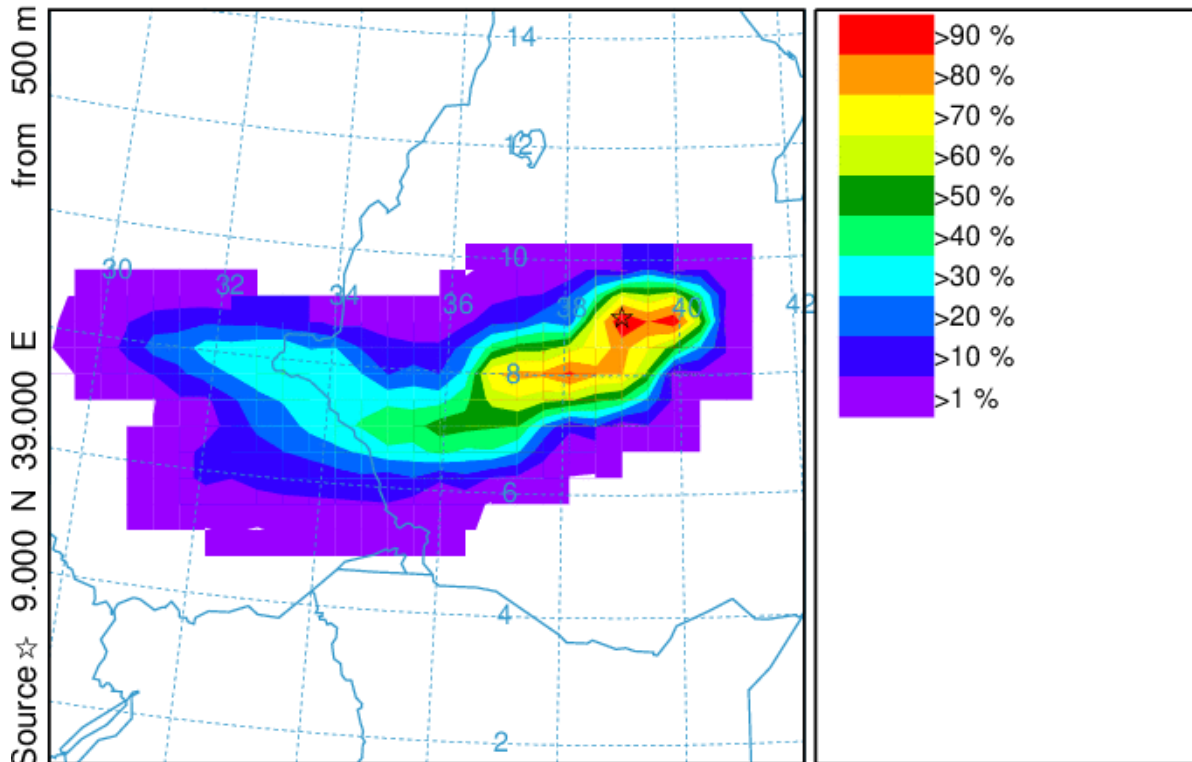


Figure 10 shows plume paths that correspond to the main regional circulation systems.

NOAA HYSPLIT MODEL - TRAJECTORY FREQUENCIES
 # trajs passing through grid sq./# trajectories (%) 0 m and 99999 m
 Integrated from 1400 29 Dec to 1100 02 Jan 26 (UTC)
 Freq Release started at 0000 00 00 (UTC)

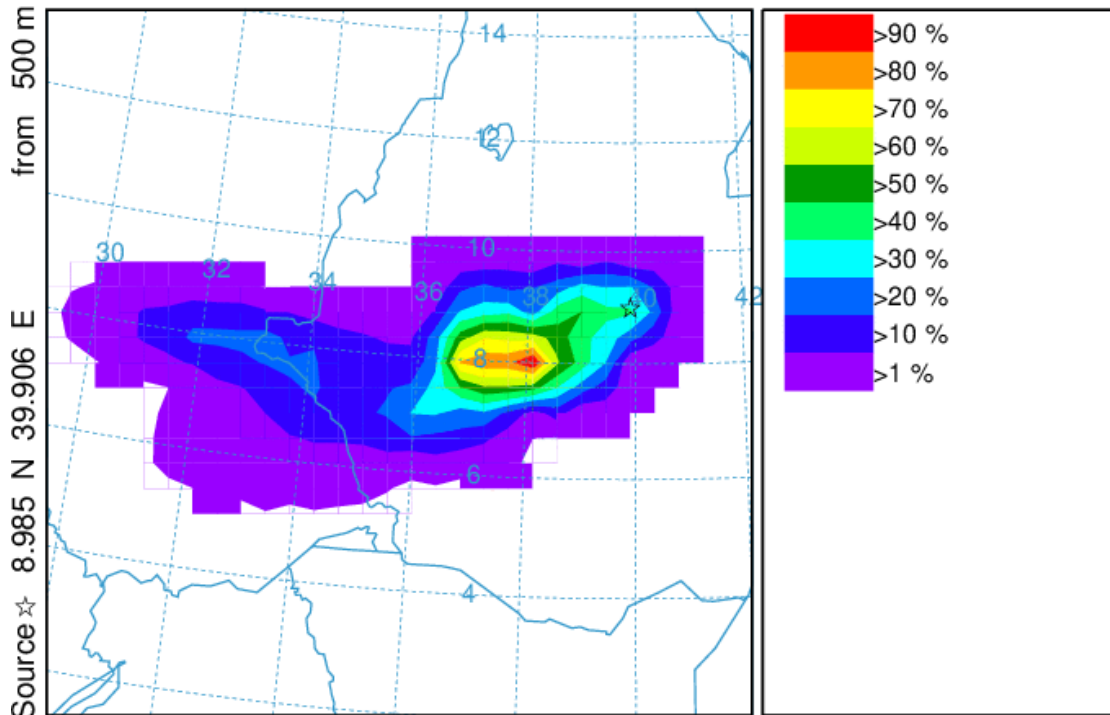


METEOROLOGICAL DATA

Job ID: 170357 Job Start: Sat Jan 24 00:33:19 UTC 2026
 Source 1 lat.: 8.985000 lon.: 39.906000 height: 500 m AGL
 Initial trajectory started: 1400Z 29 Dec 25
 Direction of trajectories: Forward Trajectory Duration: 48 hrs
 Frequency grid resolution: 1.0 x 1.0 degrees
 Endpoint output frequency: 60 per hour
 Number of trajectories used for this calculation: 16
 Meteorology: 0000Z 29 Dec 2025 - GDAS1

Figure 11 illustrates how plume impact regions can undergo substantial changes over time.

NOAA HYSPLIT MODEL - TRAJECTORY FREQUENCIES
 # endpts per grid sq./max # endpts in any grid sq. (%) 0 m and 99999 m
 Integrated from 1400 29 Dec to 1100 02 Jan 26 (UTC)
 Freq Release started at 0000 00 00 (UTC)



METEOROLOGICAL DATA

Job ID: 170357 Job Start: Sat Jan 24 00:33:19 UTC 2026
 Source 1 lat.: 8.985000 lon.: 39.906000 height: 500 m AGL
 Initial trajectory started: 1400Z 29 Dec 25
 Direction of trajectories: Forward Trajectory Duration: 48 hrs
 Frequency grid resolution: 1.0 x 1.0 degrees
 Endpoint output frequency: 60 per hour
 Number of trajectories used for this calculation: 16
 Meteorology: 0000Z 29 Dec 2025 - GDAS1

Figure (12) shows several trajectories with significant spatial dispersion.

UNDER REVIEW

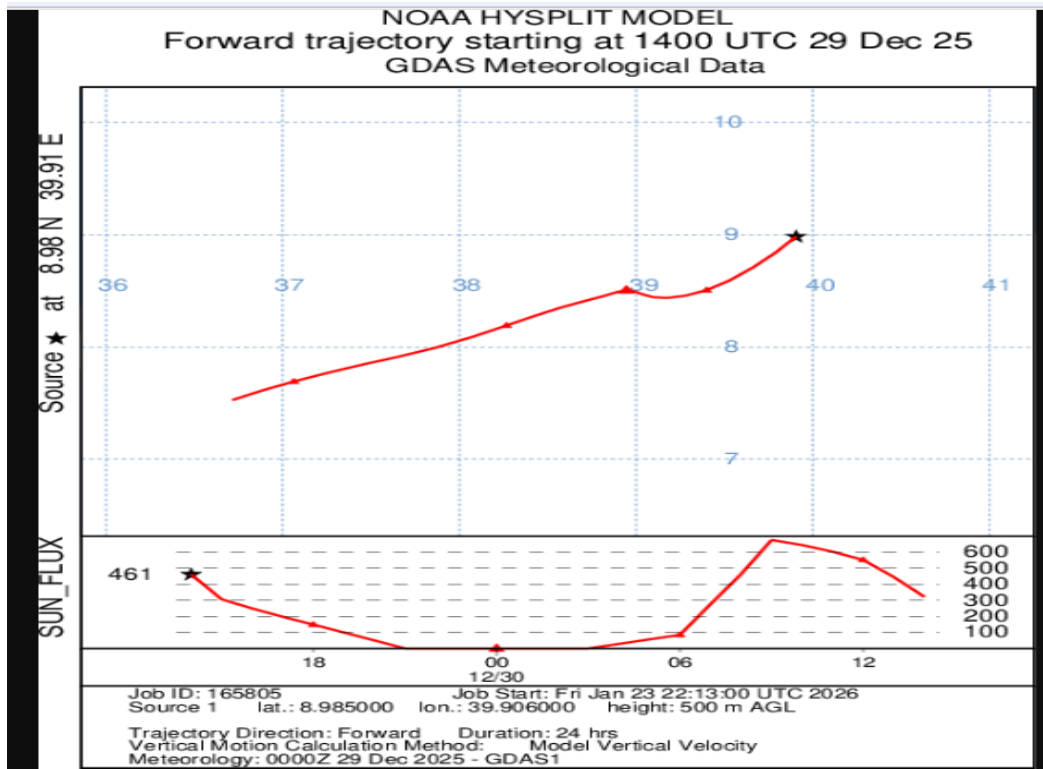
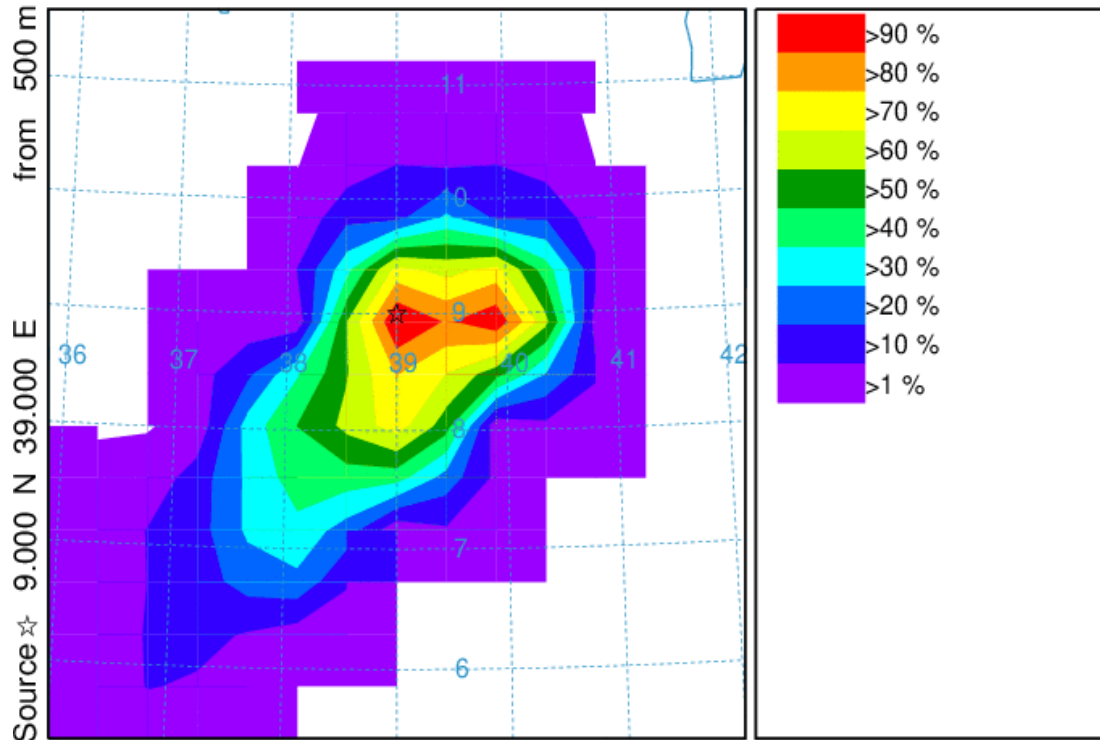


Figure (13) shows trajectories reaching distant regions well beyond the source

UNDER PEER REVIEW

NOAA HYSPLIT MODEL - TRAJECTORY FREQUENCIES
 # trajs passing through grid sq./# trajectories (%) 0 m and 99999 m
 Integrated from 1400 15 Jan to 1100 19 Jan 26 (UTC)
 Freq Release started at 0000 00 00 (UTC)

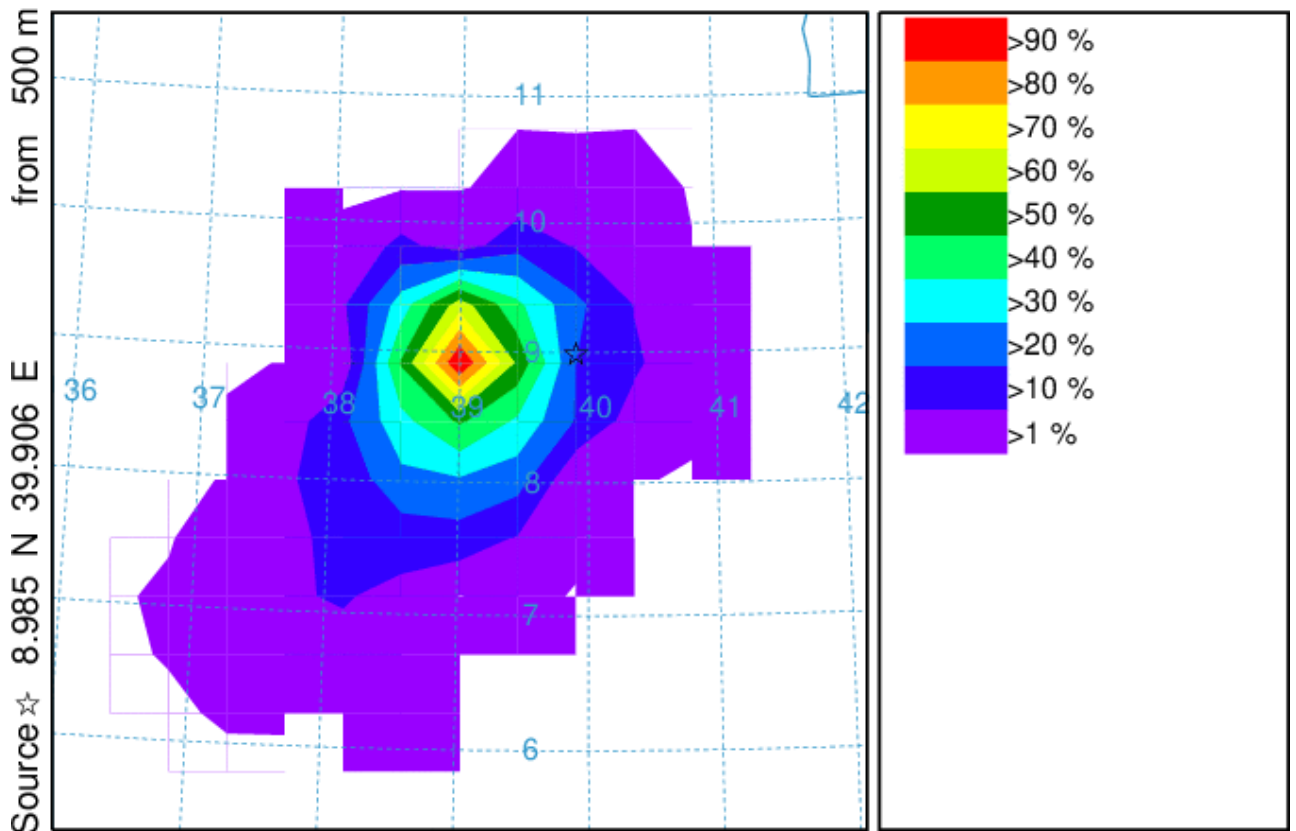


Job ID: 170729 Job Start: Sat Jan 24 00:36:47 UTC 2026
 Source 1 lat.: 8.985000 lon.: 39.906000 height: 500 m AGL
 Initial trajectory started: 1400Z 15 Jan 26
 Direction of trajectories: Forward Trajectory Duration: 48 hrs
 Frequency grid resolution: 1.0 x 1.0 degrees
 Endpoint output frequency: 60 per hour
 Number of trajectories used for this calculation: 16
 Meteorology: 0000Z 15 Jan 2026 - GDAS1

Figure 14 shows the plume paths throughout the late stages of transport.

UNDER REVIEW

NOAA HYSPLIT MODEL - TRAJECTORY FREQUENCIES
 # endpts per grid sq./max # endpts in any grid sq. (%) 0 m and 99999 m
 Integrated from 1400 15 Jan to 1100 19 Jan 26 (UTC)
 Freq Release started at 0000 00 00 (UTC)



METEOROLOGICAL DATA

Job ID: 170729 Job Start: Sat Jan 24 00:36:47 UTC 2026
 Source 1 lat.: 8.985000 lon.: 39.906000 height: 500 m AGL
 Initial trajectory started: 1400Z 15 Jan 26
 Direction of trajectories: Forward Trajectory Duration: 48 hrs
 Frequency grid resolution: 1.0 x 1.0 degrees
 Endpoint output frequency: 60 per hour
 Number of trajectories used for this calculation: 16
 Meteorology: 0000Z 15 Jan 2026 - GDAS1

Figure (15). Shows weak directional coherence and widely scattered trajectories

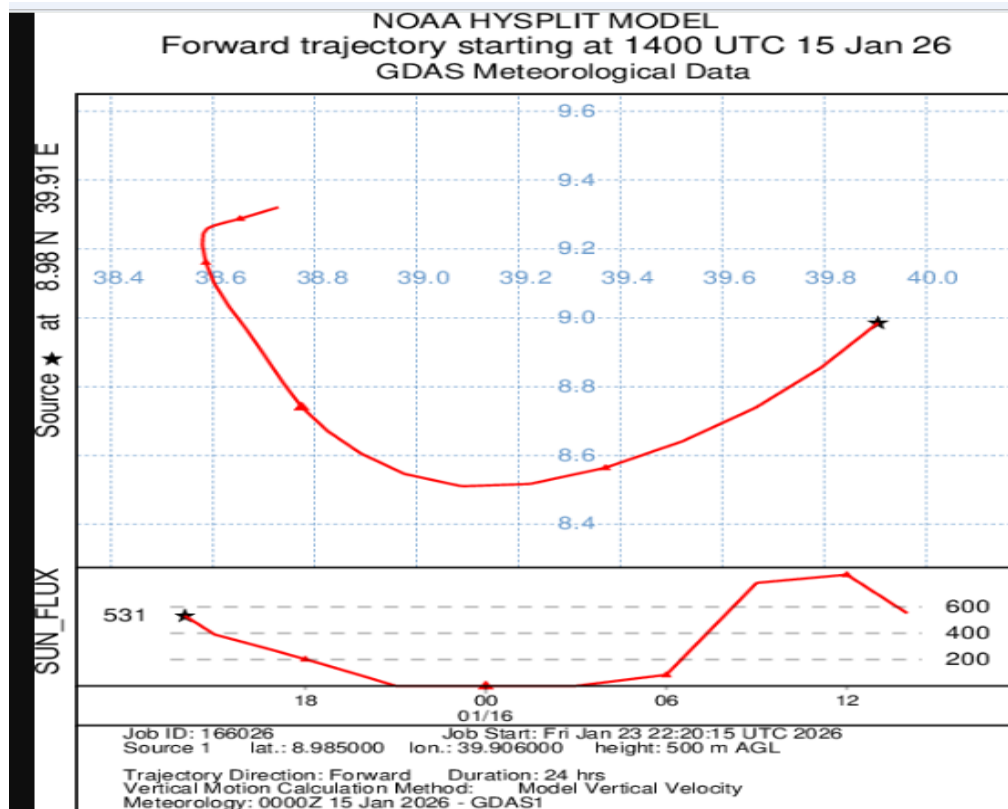


Figure (16) illustrates the volcanic plume trajectory.

Conclusion:-

According to the results of the HYSPLIT model simulation, the main physical elements controlling the temporal and spatial extent of dispersion are injection height, upper-level wind continuity, and vertical wind shear arrangement. The findings also showed that as travel time increases, directional coherence gradually declines, increasing spatial uncertainty. The findings are in full accordance with the International Atomic Energy Agency's (IAEA) recommendations for simulating atmospheric dispersion in radiological emergencies, especially with regard to the significance of figuring out injection height, examining the dispersion envelope's temporal evolution, and evaluating transboundary effects. Moreover, the findings are consistent with the techniques used by the United Nations Scientific Committee on the Effects of Atomic Radiation to describe the long-range movement of radioactive elements and evaluate the geographical and temporal fluctuations in environmental exposure patterns. The study demonstrates that, in spite of its geological origin, the behavior of the volcanic plume serves as a physical model that is comparable to the behavior of radioactive contaminants in the air. Because of this, these results can be utilized as a scientific foundation to improve the accuracy of long term dose estimation, increase the preparedness of environmental monitoring systems, and establish national and regional reaction plans to radioactive release disasters. Therefore, our study helps to close a large knowledge gap about how to combine worldwide radiation protection regulation frameworks with sophisticated numerical modeling of air dispersion .

Reference :-

- 1- World Bank (2021). climate risk country Profile – Ethiopia
- 2- Chorowicz, J. (2005). The East African rift system. *Journal of African Earth Sciences*, 43(1–3), 379–410
- 3- Barberi, F., & Varet, J. (1977). Volcanism of Afar: Small-scale plate tectonics implications. *Geological Society of America Bulletin*, 88(9), 1251–1266.
- 4- Chorowicz, J. (2005). The East African rift system. *Journal of African Earth Sciences*, 43(1–3), 379–410
- 5- Ebinger, C. J. (2005). Continental break-up: The East African perspective. *Astronomical & Geophysical Journal*, 46(2), 2.16–2.21.
- 6- Keir, D., Ebinger, C., Stuart, G., et al. (2009). Strain accommodation by magmatism and faulting as rifting proceeds to breakup. *Journal of Geophysical Research*, 114(B5).
- 7- Siebert, L., Simkin, T., & Kimberly, P. (2010). *Volcanoes of the World* (3rd ed.). University of California Press.
- 8- Holton, J. R., Haynes, P. H., et al. (1995). Stratosphere–troposphere exchange. *Reviews of Geophysics*, 33(4), 403–439.
- 9- Textor, C., Graf, H. F., Timmreck, C., & Robock, A. (2004). Emissions from volcanoes. *Journal of Geophysical Research: Atmospheres*, 109(D19).
- 10- Robock, A. (2000). Volcanic eruptions and climate. *Reviews of Geophysics*, 38(2), 191–219.
- 11- Gerlach, T. (2011). Volcanic versus anthropogenic carbon dioxide. *Eos, Transactions American Geophysical Union*, 92(24), 201–202.
- 12- Carn, S. A., Krueger, A. J., et al. (2003). Tracking volcanic sulfur dioxide clouds. *Journal of Geophysical Research*, 108(D10).
- 13- Prata, A. J., & Tupper, A. (2009). Aviation hazards from volcanoes: The state of the science. *Natural Hazards*, 51, 239–244.
- 14- Textor, C., Graf, H. F., Timmreck, C., & Robock, A. (2004). Emissions from volcanoes. *Journal of Geophysical Research: Atmospheres*, 109(D19).
- 15- Robock, A. (2000). Volcanic eruptions and climate. *Reviews of Geophysics*, 38(2), 191–219
- 16- Sparks, R. S. J., et al. (1997). *Volcanic Plumes*. Wiley
- 17- Chai, T., Crawford, B.J.B. Stunder, M.J. Pavolonis & R.R. Draxler (2017). Improving volcanic ash predictions with the HYSPLIT dispersion model by assimilating MODIS satellite retrievals. *Atmospheric Chemistry and Physics*, 17, 2865–2880.
- 18- Draxler, R.R., & G.D. Hess (1997). Description of the HYSPLIT_4 modeling system. NOAA Tech. Memo. ERL ARL-224, Silver Spring, MD: NOAA Air Resources Laboratory.

- 19-** Draxler, R.R., & G.D. Hess (1998). An overview of the HYSPLIT₄ modeling system of trajectories, dispersion, and deposition. *Aust. Meteor. Mag.*, 47, 295-308.
- 20-** Draxler, R.R. (1999). HYSPLIT₄ user's guide. NOAA Tech. Memo. ERL ARL-230. Silver Spring, MD: NOAA Air Resources Laboratory.
- 21-** Stein, A.F., R.R. Draxler, G.D. Rolph, B.J.B. Stunder, M.D. Cohen & F. Ngan (2015). NOAA's HYSPLIT Atmospheric Transport and Dispersion Modeling System, *Bull. Amer. Meteor. Soc.*, 96, 2059-2077, <http://dx.doi.org/10.1175/BAMS-D-14-00110>.
- 22-** La Rosa, A., et al. (2025) Segmented dike intrusion linked to multi-level magma storage during and before the 2025 eruption at Erta Ale (East Africa). *Frontiers in Earth Science*, 13:1719687.
- 23-** NASA Earth Observatory (2023, December 3) The Smoking Mountain. Accessed December 3, 2025.
- 24-** Simon Carn, via Bluesky (2025, November 23) An explosive eruption of HayliGubbi volcano. Accessed December 3, 2025.
- 25-** Sparks, R. S. J., Bursik, M. I., Carey, S. N., et al. (1997). *Volcanic Plumes*. Wiley
- 26-** Holton, J. R., & Hakim, G. J. (2013). *An Introduction to Dynamic Meteorology* (5th ed.). Academic Press
- 27-** Woods, A. W. (1988). The fluid dynamics and thermodynamics of eruption columns. *Bulletin of Volcanology*, 50, 169–193.
- 28-** Stull, R. B. (1988). *An Introduction to Boundary Layer Meteorology*. Springer.
- 29-** Bostan, D.-C., Miclăuș, I.-M., Apetroaie, C., Voiculescu, M., Timofte, A., & Cazacu, M.-M. (2023). Long-Range Transport Analysis Based on Eastern Atmospheric Circulation and Its Impact on the Dust Event over Moldavia, Romania in August 2022. *Atmosphere*, 14(9), 1366.
- 30-** Kesti, J., O'Connor, E. J., Hirsikko, A., Backman, J., Filioglou, M., Sundström, A.-M., Tonttila, J., Lihavainen, H., Korhonen, H. (2024). How horizontal transport and turbulent mixing impact aerosol particle and precursor concentrations at a background site in the UAE. *Atmospheric Chemistry and Physics*, 24, 9369–9386.
- 31-** Rööslä, T., Rantanen, M., & Prank, M. (2022) "Sensitivity of atmospheric Lagrangian dispersion model results to meteorological input data resolution." *Atmospheric Chemistry and Physics*, 22, 12789–12807.
- 32-** Kumar, A., Lee, H., & Gadde, R. R. (2023) "Modeling atmospheric transport of volcanic ash: Assessing dispersion, advection, and uncertainties."
- 33-** Sprigg, W. A., Prata, A. T., & Webley, P. W. (2022) "Synoptic-scale influences on volcanic ash dispersion: A case study using forward and backward trajectory ensembles.
- 34-** Rabitz, F., Prank, M., & Belova, M. (2023) "Lagrangian trajectory ensembles and atmospheric variability: implications for long-range transport uncertainty."
- 35-** Stohl, A., et al. (2023) "Long-range transport in the troposphere — mechanisms, variability and impacts." *Atmospheric Chemistry and Physics*, 23, 3457–3485.

- 36-** Natale, A., Sapiano, M. R. P., & Prasad, A. K. (2023). Changing synoptic conditions and their effect on aerosol transport pathways over Africa. *Atmospheric Research*, 289, 106679.

UNDER PEER REVIEW IN IJAR